- 1 Receptor CDCP1 is a potential target for personalized imaging and treatment of
- 2 poor outcome HER2⁺, triple negative and metastatic ER⁺/HER2⁻ breast cancers
- 3 Madeline Gough^{1,2}, Kayden KX. Kwah^{1#}, Tashbib Khan^{1#}, Saikat Ghosh¹, Biao Sun¹,
- 4 Catherine YJ. Lee¹, Kamil A. Sokolowski³, Brian WC. Tse³, Lashith Wickramasuriya¹,
- 5 Kaltin Ferguson^{1,2}, Rebecca Rogers^{1,2}, Justin B. Goh⁴, Nicholas L. Fletcher^{4,5,6}, Zachary
- 6 H. Houston^{4,5,6}, Kristofer J. Thurecht^{4,5,6}, Laura J. Bray⁷, Cheng Liu^{2,8}, Christopher
- 7 Pyke², Elgene Lim⁹, Cameron E. Snell^{8,10}, Yaowu He¹, John D. Hooper^{1*} and Thomas
- 8 Kryza^{1,8}*
- 9 1. Mater Research Institute The University of Queensland, Translational Research
- 10 Institute, Woolloongabba, QLD, Australia.
- 11 2. Mater Health Services, South Brisbane, QLD, Australia.
- 12 3. Preclinical Imaging Facility, Translational Research Institute, Woolloongabba, QLD,
- 13 Australia
- 14 4. Australian Institute for Bioengineering and Nanotechnology, The University of
- 15 Queensland, St. Lucia, Queensland, Australia
- 16 5. Centre for Advanced Imaging, The University of Queensland, St. Lucia, Queensland,
- 17 Australia
- 18 6. Australian Research Council Centre of Excellence in Convergent Bio-Nano Science
- and Technology, The University of Queensland, Australia.
- 20 7. School of Mechanical, Medical and Process Engineering, Faculty of Engineering,
- 21 Queensland University of Technology, Brisbane, QLD, Australia
- 22 8. Faculty of Medicine, The University of Queensland, St. Lucia, QLD, Australia
- 23 9. Garvan Institute of Medical Research, Sydney, NSW, Australia
- 24 10. Peter MacCallum Cancer Centre, Melbourne, VIC, Australia
- 25 Corresponding authors: Thomas Kryza, Mater Research Institute The University of
- 26 Queensland, Translational Research Institute, Woolloongabba, Qld 4102, Australia; E-
- 27 mail: uqtkryza@uq.edu.au; **John Hooper**, Mater Research Institute The University of
- 28 Queensland, Translational Research Institute, Woolloongabba, Qld 4102, Australia; E-

29 mail: john.hooper@mater.uq.edu.au. #These authors contributed equally to the 30 manuscript.

ABSTRACT

31

32

33

34

35

36

37

38

39

40

41

42

43

44

45

46

47

48

49

50

51

52

53

54

55

56

Purpose: Receptor CUB-domain containing- protein 1 (CDCP1) was evaluated as a target for detection and treatment of breast cancer.

Experimental Design: CDCP1 expression was assessed immunohistochemically in tumors from 423 patients (119 triple-negative breast cancer (TNBC): 75 HER2⁺: 229 ER⁺/HER2⁻ including 228 primary tumors, and 229 lymph node and 47 distant metastases). Cell cytotoxicity induced in vitro by a CDCP1-targeting antibody-drug conjugate (ADC), consisting of the human/mouse chimeric antibody ch10D7 and the microtubule disruptor monomethyl auristatin E (MMAE), was quantified. including in combination with HER-targeting ADC T-DM1. Detection of CDCP1expressing primary and metastatic xenografts in mice was examined by PET-CT imaging using ⁸⁹zirconium-labelled ch10D7 (⁸⁹Zr-ch10D7). The impact of ch10D7-MMAE on tumor burden and survival in vivo, including in combination with T-DM1, was quantified in cell line and patient-derived xenograft mouse models.

Results: CDCP1 is expressed predominantly on the surface of malignant cells of 70% of TNBCs, 80% of HER2⁺ tumors, and increases in ER⁺/HER2⁻ tumors from 44.9% in primary tumors to 56.4% in lymph node metastases and 74.3% in distant metastases. PET-CT imaging with ⁸⁹Zr-ch10D7 is effective for the detection of primary and metastatic CDCP1-expressing TNBCs in mice. ADC ch10D7-MMAE kills CDCP1-expressing cells *in vitro* and controls primary and metastatic TNBC xenografts in mice, conferring significant survival advantages over chemotherapy. It compares favorably to T-DM1 *in vivo*, and ch10D7-MMAE combined with T-DM1 showed the most potent efficacy, markedly reducing tumor burden of CDCP1⁺/HER2⁺ xenografts and prolonging mouse survival, compared with T-DM1 or ch10D7.

Conclusions: CDCP1-directed molecular imaging has potential to identify aggressive breast cancers for CDCP1-targeted treatment.

Translational Relevance

CDCP1 is a receptor enriched on the surface of the malignant cells of 56.4-80% of aggressive breast cancers, including TNBCs, HER2⁺ and metastatic ER⁺/HER2⁻ tumors. Human/mouse chimeric anti-CDCP1 antibody ch10D7 is effective at delivering radionuclide and drug payloads for detection and treatment of disease-relevant models of breast cancer. There is potential for PET-CT imaging with radio-labelled CDCP1-targeted agents to be used to determine the optimal clinical regimen for selection of breast cancer patients for treatment with a CDCP1-targeted therapeutic agent.

83

84

85

86

87

88

89

90

91

92

93

94

95

96

97

98

99

100

101

102

103

104

105

106

107

108

109

110

111

112

INTRODUCTION

Breast cancer is the second most commonly diagnosed cancer worldwide, with over 2.3 million new cases in 2022, and the leading cause of cancer related death in women, and it is predicted this burden will continue to rise [1]. It is a heterogeneous malignancy, and despite significant therapeutic advancements, effective treatment options are still lacking in triple negative breast cancer (TNBC), metastatic estrogen receptor positive (ER⁺) tumors that are human epidermal growth factor receptor 2 (HER2) negative, and treatment refractory/metastatic HER2-positive (HER2⁺) disease [2-4]. Management of these aggressive subtypes would benefit from molecular imaging agents, allowing non-invasive tumor staging and identification of patients for molecularly-targeted treatments [5, 6].

Already prominent in the clinical management of several aggressive breast cancer subtypes, are precision medicines targeting cell surface receptors, in particular HER2 and more recently Trop-2 [7, 8]. Eleven targeted ADCs have FDA approval with two, Trastuzumab Emtansine (T-DM1) and Trastuzumab Deruxtecan (T-DXd), available for metastatic HER2⁺ breast cancer, with the second of these effective for patients with low and heterogeneous HER2 expression [9]. TNBC currently has only one approved ADC, Trop-2-targeting sacituzumab govitecan, but responses are generally not durable [10]. Selection of patients for treatment with precision medicines can be guided by immunohistochemical assessment of target expression in invasively collected specimens (biopsies or tumors collected at the time of primary resection) [3, 11]. For example, HER2 expression levels in tumors, assessed by immunohistochemistry, are used to clinically predict breast cancer response to HER2-targeted therapies [12-15]. Scoring is performed semi-quantitatively assessing both the proportion of tumor cells with membrane HER2 signal and signal intensity [12, 16, 17]. However, a weakness is that such immunohistochemical approaches do not account for intra- or inter-tumor heterogeneity or the impact of subsequent lines of treatment on tumor target expression [7, 11] Molecular imaging has the potential to improve patient selection for treatment with receptor targeting precision medicines. By using theranostic agents that bind with high affinity to the target to deliver an energy-emitting payload, the molecular imaging

modality positron emission tomography–computed tomography (**PET-CT**), is able to define sites and levels of expression and stratify patients for subsequent treatments with therapeutic radionuclides or ADCs [18].

The 135 kDa transmembrane glycoprotein receptor CUB-domain containing protein 1 (CDCP1) is emerging as a potential additional precision medicine target for several breast cancer subtypes based on its increased expression in breast tumors compared with normal tissues, and its function in molecular and cellular processes associated with progression of breast cancer [19-28]. Analysis of 224 poorly-defined normal and malignant specimens showed expression of CDCP1 in ~24% of primary tumors increasing to ~40% of metastases versus ~5% of normal breast samples [19]. Sub-analysis indicated that elevated CDCP1 expression increased in tumors that had highest levels of HER2 (score 3+) from 12% in primary tumors to 30% in metastases [19]. In a cohort of 35 untyped invasive breast carcinomas, 57.5% were medium to high CDCP1 expressers [29], while in two cohorts of 65 and 100 primary TNBCs, 57% displayed CDCP1 positivity on ≥ 10% of malignant cells [20, 21]. The poor histological definition of the breast cancer patient cohorts, and variation in antibodies and protocols used in these studies, is hampering assessment of CDCP1 as a valid molecular target for breast cancer.

We have previously reported a semi-quantitative immunohistochemical method integrating staining intensity and the proportion of positive cancer cells to assess CDCP1 expression in cancer [29]. It has been used to identify the proportion of bladder, colon, lung, pancreatic, prostate and breast (including the 35 untyped invasive breast carcinomas mentioned above) cancers that express CDCP1 [29]. The results demonstrate that a significant majority of patients display medium or high CDCP1 expression in tumors (bladder 58.7%, colon 97.2%, lung 60.6%, pancreatic 88.6%, prostate 43.2%, breast 57.1%) [29]. CDCP1 levels for these tumors were well above those quantified by us in 34 normal tissues, suggesting that tumors with elevated CDCP1 expression could be targeted with a CDCP1-targeted therapy without dose-limiting off-tumor toxicity [29].

In the present study, to more accurately evaluate CDCP1 as a potential breast cancer target, we quantified its protein expression by immunohistochemistry in well-defined patient cohorts allowing us to estimate the proportion of patients in poor outcome TNBC, HER2+ and metastatic ER+/HER2- groups who could potentially benefit from CDCP1-targeting agents. In addition, we performed quantitative preclinical PET-CT imaging of cell line and patient-derived xenograft mouse models, using zirconium-89 (89Zr) labelled human/mouse chimeric anti-CDCP1 antibody ch10D7 [29, 30], to assess the utility of targeting CDCP1 for molecular imaging-based detection of primary and metastatic breast cancer. Furthermore, we evaluated the efficacy *in vitro* and in mouse models of cytotoxin-loaded antibody ch10D7, including in combination with a HER2-targeting ADC. The data support the potential of ch10D7 as a theranostic agent for identification of CDCP1-expressing HER2+, TNBC and ER+/HER2- breast cancer that are suitable for CDCP1-directed treatment.

METHODS AND MATERIALS

Immunohistochemistry

The use of patient specimens was approved by the Mater Health Services Human Research Ethics Committee (approval number: PRGRPT/MML/70016). CDCP1 immunohistochemistry was performed as previously described [31] on tissue microarrays containing 120 primary TNBC (one core per case; US Biomax BR1301a; Derwood, MD), 75 HER2⁺ invasive ductal carcinoma (two cores per case; US Biomax BR1506) and 229 ER⁺/HER2⁻(228 primary, 229 lymph node metastases and 47 distant metastases) cases [32]. Deparaffinized sections, blocked for endogenous peroxidases, were subjected to antigen retrieval in EDTA Buffer (pH 8.0) at 110°C for 15 minutes, followed by overnight incubation at 4°C with anti-CDCP1 antibody 4115 (1:100, RRID:AB_2078818). Detection was performed using the Novolink Detection Kit (Leica Biosystems, Mount Waverley, Australia) following manufacturer's instructions. The following antibodies were used from Ventana (Medical Systems Inc., Tucson, Arizona) and were stained on the Ventana BenchMark Ultra (Roche Diagnostics, North Ryde, Australia, RRID:SCR_025506): CONFIRM anti-Estrogen (ER) (Ventana, clone (SP1,

173 RRID:AB 2335977), CONFIRM anti-Progesterone (PR)(Ventana, clone 1E2. 174 RRID:AB_2335976), PATHWAY HER2 (Ventana, clone 4B5, RRID:AB_2335975), 175 CONFIRM anti-Ki67 (Ventana, clone 30-9, RRID:AB_2631262), Ventana HER2 Dual 176 ISH DNA Probe Cocktail, according to manufacturer's instructions. Staining was 177 assessed and CDCP1 signal was scored by an experienced breast pathologist (C.E.S.) 178 using a semi-quantitative two parameter system for intensity (0, no staining; 1, weak; 2, 179 moderate; or 3 strong) and the percentage of stained cells (0 to 100%). The product of 180 the two parameters generated an overall score of 0 to 300 with scores segregated into 181 negative (0), low (0-99), moderate (100-199) and strong (200-300) groups.

Cell lines and culture

182

183

184

185

186

187

188

189

190

191

192

193

194

195

196

197

198

199

200

201

202

203

Breast cancer cell lines MDA-MB-231 (RRID:CVCL 0062), MDA-MB-468 (RRID:CVCL 0419), (RRID:CVCL 0418), MDA-MB-453 MDA-MB-361 (RRID:CVCL 0620), SKBR3 (RRID:CVCL 0033), T47D (RRID:CVCL 0553), MCF7 (RRID:CVCL_0031), BT474 (RRID:CVCL_0179) and HCC1954 (RRID:CVCL_1259) were from American Type Culture Collection (Manassas, VA), from a range of breast cancer subtypes, including ER⁺, HER2⁺ and TNBC [33-39]. Cell lines were regularly tested for mycoplasma contamination and authenticated by STR profiling. Three normal human breast epithelial cell lines derived from patient tissues (HMEC #6, #8 and #13) were cultured in the Mammary Epithelial Cell Growth Medium Bulletkit (Lonza, Basel, Switzerland) at 37°C in a humidified 5% CO₂ atmosphere as previously described [40]. All ATCC cell lines were cultured in Dulbecco's Modified Eagle Medium supplemented with 10% fetal bovine serum (FBS) and 50 U/ml penicillin streptomycin media at 37°C in a humidified 5% CO₂ atmosphere. To avoid cleavage of cell surface proteins, cultures were passaged non-enzymatically with Versene (0.48mM EDTA in PBS, pH 7.4). MDA-MB-231 (RRID:CVCL_0062) and HCC1954 (RRID:CVCL_1259) cells were labelled with luciferase, generating MDA-MB-231-luc and HCC1954-luc cells, using a previously described lentivirus-based expression construct and selection of stably transduced cells in Blasticidin containing media (1 µg/ml)[41]. Labelling efficiency was assessed by plating cells in duplicate in serial dilutions and measuring luminescence on an IVIS Bioluminescence System (RRID:SCR 025239), using LivingImage software (Caliper Life Sciences, Mountain View, CA, RRID:SCR_014247).

Antibody-drug conjugation

Conjugation of microtubule disrupting cytotoxin monomethyl auristatin E (MMAE) to ch10D7 and IgG1k was performed as previously described [29]. Briefly, antibody inter-chain disulfides were first partially reduced using DTT (10 nM, 15 min, 37°C) to generate free thiols, which were reacted with excess maleimide activated MC-VC-PAB-MMAE in 10% DSMO for 2 h at 4°C (on ice). Impurities were removed from crude reaction mixtures by filtering through PD-10 Sephadex G-25 columns (Cytiva, Marlborough, MA), then ADCs were purified by size exclusion chromatography through a HiLoad 26/600 Superdex 200 pg column on an ÄKTA go system (Cytiva). Eluted fractions were analyzed by UV absorbance spectroscopy at 280 nm, then ADC containing fractions were concentrated using Amicon 10K MWCO ultracentrifugation columns (Merck, Bayswater, Australia). ADC purity was evaluated using the ÄKTA evaluation suite and by Coomassie-stained SDS-PAGE gel analysis in comparison with the unlabelled antibodies. DAR was determined by hydrophobic interaction liquid chromatography-mass spectrometry as previously described [42].

In vivo testing of ADCs

Mouse experiments were approved by the University of Queensland Animal Ethics Committee (approvals 2022/AE000594 and 2022/AE000659). For orthotopic assays, female NSG mice (RRID:BCBC_4142, 6-7/group) were inoculated in the mammary fat pad with cells (TNBC MDA-MB-231-luc or HER2+ MDA-MB-453; 1×10⁶ in PBS) or 1 mm³ pieces of three published patient-derived xenograft (PDX) models (TNBC ELX 11-26, HCI-010; HER2+ ELX 14-06A) [43, 44] or a new TNBC PDX BB-091 generated from the primary breast tumor of a 46 year old women and validated by histological assessment by an experienced breast pathologist (C.E.S.). Tumor burden was quantified for luciferase-labelled cell xenografts by weekly bioluminescent imaging on an IVIS Spectrum system as described [42], and for the PDX by calliper measurement twice weekly. For MDA-MB-453 cell xenografts, mice were randomized when bioluminescent signal reached >10⁹p/s/cm²/sr. For PDX ELX 11-26 mice were randomized when average tumor volume reached ~50 mm³ and for MDA-MB-453 cell xenografts and PDX ELX 14-06A when average tumor volume reached ~150 mm³. Mice with MDA-MB-453 cell xenografts were then treated intravenously (i.v.) every two weeks

with IgG-MMAE, ch10D7-MMAE, T-DM1 (5 mg/kg), the combination of ch10D7-MMAE and T-DM1 (total of 5/kg or 10 mg/kg, fortnightly) or vehicle (100 µl; weekly). Mice carrying PDX ELX 11-26 received three i.v. treatments once every two weeks with ch10D7-MMAE (5 mg/kg) or vehicle (100 µl; weekly), and mice carrying PDX ELX 11-26 received three i.v. treatments once every two weeks with ch10D7-MMAE (5 mg/kg), T-DM1 (5 mg/kg), or the combination of ch10D7-MMAE and T-DM1 (total of 5 or 10 mg/kg). Mice were culled when tumor burden or animal discomfort exceeded ethically approved limits, with survival examined by Kaplan-Meier analysis as described [42].

235

236

237

238

239

240

241

242

243

244

245

246

247

248

249

250

251

252

253

254

255

256

257

258

259

260

261

262

263

264

265

For metastasis assays, tumor burden of female NSG mice (RRID:BCBC 4142, 9-10/group,) injected i.v. with TNBC MDA-MB-231-luc or HCC1954-luc cells (1×10⁶ in PBS) was quantified by weekly bioluminescent imaging. Once the average bioluminescent signal reached >10⁷ p/s/cm²/sr, mice were randomised then mice carrying MDA-MB-231-luc cell xenografts were treated i.v. weekly with vehicle (100 µl PBS), carboplatin (30 mg/kg), IgG-MMAE (5 mg/kg), ch10D7-MMAE (5 mg/kg), IgG-MMAE and carboplatin (5 mg/kg and 30 mg/kg respectively) or ch10D7-MMAE and carboplatin (5 mg/kg and 30 mg/kg respectively). In this metastasis model, the dosing regimen was escalated from every two weeks, which was employed for orthotopic xenografts, to weekly administration because tumor colonization in the lungs after intravenous delivery of malignant cells leads to more rapid morbidity and mortality than orthotopic xenografts. Mice inoculated with HCC1954-luc cells were treated i.v. every two weeks with vehicle (100 µl PBS), ch10D7-MMAE (5 mg/kg), T-DM1 (5 mg/kg), or the combination of ch10D7-MMAE and T-DM1 (each 5 mg/kg). On day 50 after inoculation of cells, when the first animal displayed tumor bioluminescence signal of >10¹⁰, tumor burden was quantified by bioluminescent imaging. At that time, the animal with the highest signal was sacrificed from each treatment group. Lung tumor burden was quantified ex vivo after submersion of lungs in a solution of D-luciferin with bioluminescence signal quantified using LivingImage software (RRID:SCR_014247) on an IVIS spectrum (RRID:SCR 014247). Harvested lungs were fixed, processed in increasing concentrations of ethanol followed by a two-hour treatment with hexamethyldisilazane and air drying, then lung malignancy was defined by high resolution microCT imaging on a SkyScan 1272 system (software version 1.4, Bruker,

Kontich, Belgium; 13 μm pixel size, 50 kV voltage, 200 μA current, 170 ms exposure time, no filter, averaging of 3, 0.25° rotation step around 360° of the sample), using NRecon reconstruction software (Version 1.7.3, Bruker), and a Feldkamp algorithm with ring artefact and beam hardening correction, with 3D Visualisations generated using CTVox (Version 3.3.0 Bruker). For the remaining animals, mice were culled when tumor burden or animal discomfort exceeded ethically approved limits, with survival examined by Kaplan-Meier analysis as described [36].

PET-CT imaging

266

267

268

269

270

271

272

273

274

275

276

277

278

279

280

281

282

283

284

285

286

287

288

289

290

291

292

293

294

Antibody labelling with the metal chelator deferoxamine then the positronemitting radionuclide ⁸⁹Zr was as previously described [29, 31, 42, 45]. Thin layer and high-performance liquid chromatography (Agilent, Mulgrave, Australia) were performed to quantify yield and purity of 89Zr-ch10D7. Injected radioactivity was calculated by subtracting the residual radioactivity in the syringe after injection, measured using a Biodex Atomlab 500 Dose Calibrator (Shirley, New York), from the preinjection reading. PET-CT imaging was performed on female NSG mice (RRID:BCBC 4142) carrying mammary fat pad (orthotopic) or metastatic breast cancer xenografts (cell lines inoculated via the lateral tail vein). After establishment of xenografts, mice (4-8 mice/group) were injected intravenously with ⁸⁹Zr-ch10D7 (~2.0 MBg; 0.1 ml) and, 24 h earlier, unlabelled ch10D7 or PBS to assess the specificity of the agent in vivo for CDCP1 expressing cells. PET-CT imaging was performed on isoflurane anaesthetised mice after 24, 48 and 72 h, and for some assays 120 h, using Molecubes β-Cube and X-Cube Systems (Molecubes, Gent, Belgium). PET acquisition (20 minutes; static emission) was performed, and images were reconstructed using an ordered-subset expectation maximization (OSEM2D) algorithm, with CT attenuation correction. The CT scan parameters were 50 kV, 75 µA, 480 exposures at 85 ms each, continuous helical rotation, and images using ISRA algorithm. PET-CT data was analysed and visualised using PMOD software v4.206 (PMOD Technologies, Fällanden, Switzerland, RRID:SCR 016547). After 120 h, ex vivo biodistribution analysis was assessed on blood and cleaned harvested tumor and organs, which were weighed and radioactivity quantified using a Wizard 2480 gamma counter (Revvity, Waltham, MA) and presented as %ID/g of tissue or blood (after decay and detector efficiency corrections).

Statistical analyses

Data were analyzed using GraphPad Prism 8 (GraphPad Software, La Jolla, CA, RRID:SCR_002798). Results are presented as means \pm standard deviation (SD) for *in vitro* assays and \pm standard error of the mean (SEM) for mouse assays. The Mann-Whitney test was used for comparing two groups from *in vitro* assays. For PET-CT imaging assays, statistical significance between different groups was performed using a two-way ANOVA test. For mouse treatment assays, the Kruskal-Wallis test was used for comparisons involving more than two groups, while survival was compared using Logrank Gehran-Breslow Wilcoxon Chi² test. Significance values are represented in graphs as $*P \le 0.05$, $**P \le 0.01$, $***P \le 0.001$ and $*****P \le 0.0001$.

Availability of data and materials

The datasets analysed in the study as well as the raw data corresponding to the experiments presented are available from corresponding authors Dr Thomas Kryza and Professor John D. Hooper on reasonable request.

RESULTS

CDCP1 is elevated in TNBC and HER2⁺ and metastatic ER⁺/HER2⁻ breast cancers

To more accurately define the proportion of breast cancer subtypes and patients that could benefit from CDCP1 targeted agents, we examined by immunohistochemistry using a validated antibody [41, 46], CDCP1 protein expression in tissue-microarrays containing specimens from 423 patients (229 ER+/HER2-, 75 HER2+, 119 TNBC). CDCP1 expression was determined by multiplying CDCP1 staining intensity across the malignant component of the specimen (0, none; 1, weak; 2, moderate; or 3 strong) and the percentage of malignant cells positive for CDCP1 expression (0-100%) with the product, from 0 to 300, separated into expression brackets of 0 (none), 1-100 (low), 101-200 (medium) and 201-300 (high). In the evaluable ER+/HER2- cohort of 228 primary tumors, 229 lymph node and 47 distant metastases, a significant majority had

medium or high CDCP1 expression with the proportion increasing as disease progressed from 44.9% in primary tumors to 56.4% in lymph node metastases (P≤0.01) to 74.3% in distant metastases ($P \le 0.001$) (**Fig. 1A and B** *left*). Comparison of expression in matched specimens, with examples displayed for case 80, 151 and 195 (Fig. 1C), indicated that CDCP1 is significantly upregulated in metastases from individual patients (P=0.0127, **Fig. 1B** *middle*). In the most clinically challenging cohort of ER⁺/HER2⁻ cases, distant metastases, 80% (n=12) had increased CDCP1 expression in the metastasis (Fig. 1B right). In the HER2⁺ cohort of 75 evaluable cases CDCP1 expression (Fig. 1D) was at medium levels (score 101-200) in 41.3% of tumors, high (score 201-300) in 38.7%, with only 20% displaying low CDCP1 (score 0-100) levels (Fig. 1E). No significant associations were noted between CDCP1 level and age, grade, stage, TNM or histological subtype (median age 49 years, 29-79 years; 98.5% were Grade 2 or higher; 44.7% were Stage III or higher). In the TNBC cohort of 119 evaluable cases CDCP1 expression (Fig. 1F) was at medium levels (score 101-200) in 25.4% of tumors, high in 44.3% with 30.3% displaying low CDCP1 expression (Fig. 1G). There was no significant association between CDCP1 expression and age, stage, grade, TNM or histological subtype (median age 50 years, 31-86 years; 41.1% were Grade 3; 17.6% were stage of III or higher). These results indicate that a significant majority of ER⁺/HER2⁻, including metastases, and HER2⁺ breast cancers and TNBCs express receptor CDCP1 at levels that could be targeted for detection and/or treatment of these malignancies.

325

326

327

328

329

330

331

332

333

334

335

336

337

338

339

340

341

342

343

344

345

346

347

348

349

350

351

352

353

354

355

CDCP1 targeting ADC ch10D7-MMAE is effective *in vitro* against breast cancer cell lines

We next evaluated CDCP1 as a breast cancer treatment target in nine malignant and three non-malignant cell lines *in vitro* including the TNBC lines MDA-MB-231 and MDA-MB-468 and the HER2⁺ lines HCC1954, MDA-MB-361, MDA-MB-453, SKBR3 and BT474. As assessed by western blot, immunofluorescent staining and flow cytometry analysis, two of the malignant cell lines had negligible levels of CDCP1 (MCF7, SKBR3) and all three non-malignant lines did not express CDCP1 while the remaining seven breast cancer lines displayed low to high levels of CDCP1 (**Fig. 2A** and **Supplementary Fig. S1**). CDCP1 was targeted using an ADC consisting of

antibody ch10D7 linked to the potent microtubule disrupting cytotoxin MMAE [29]. ch10D7-MMAE had a DAR of 4.7, as determined by hydrophobic interaction liquid chromatography-mass spectrometry analysis, and was >98% pure as demonstrated by size exclusion chromatography analysis (Supplementary Fig. S2). ADC efficacy is dependent on receptor-mediated cellular internalization followed by release of the payload within the cell cytoplasm to induce target cell death [47]. Confocal microscopy analysis of CDCP1/HER2-expressing HCC1954 breast cancer cells revealed that within five minutes of commencing treatment, ch10D7 clustered on the cell surface had begun to be internalized, with cytoplasmic signal for the antibody gradually increasing during the 8 h treatment period (Fig. 2B pink). Internalization of ch10D7 induces degradation of CDCP1 as indicated by western blot analysis of lysates from HCC1954 cells showing reduced levels of full-length 135 kDa CDCP1 and 70 kDa CDCP1-CTF 24 h after commencing ch10D7 treatments with re-expression of 135 kDa CDCP1 apparent at 48 h (Fig. 2C). The levels of CDCP1-FL expressed by triple negative cell line, MDA-MB-468, were significantly reduced after 24 h treatment with ch10D7, with reduced expression sustained out to 48 h (Fig. 2C).

We next assessed the in *vitro* anti-proliferative effects of increasing concentrations of CDCP1-targeting ADC on 12 breast-derived cell lines with increasing concentrations of ch10D7-MMAE. As shown in **Figure 2D**, CDCP1 expressing cells are generally responsive to the cytotoxic effects of the ADC whereas non-expressing cells are not (**Fig. 2D**). The equimolar control treatments ch10D7, IgG-MMAE, or MC-VC-MMAE did not impact growth of ch10D7-MMAE responsive cells (Supplementary **Fig. S3**). As shown in **Fig. 2E**, graphical comparison of the concentration of ch10D7-MMAE that reduced total cell growth by 50% (IC50) versus cell surface expression of CDCP1 (antibodies/cell), indicated that the most responsive cells were those expressing CDCP1 at a threshold above 27,000 antibodies/cell (MDA-MB-231, -468 and 361, and HCC1954)(**Supplementary Fig. S1A**) while cells with low or negligible levels of cell surface CDCP1, including three non-malignant breast lines were largely unresponsive to ch10D7-MMAE (SKBR3, MCF7 and HMEC #6, #8 and #13). Three CDCP1-expressing cell lines with cell surface expression below the threshold of >27,000 antibodies/cell (**Supplementary Fig. S1A**) displayed intermediate responsiveness to

ch10D7-MMAE (T47D, 22,800 antibodies/cell, IC50 90.47 ng/ml; MDA-MB-453, 27,000 antibodies/cell IC50 43.31 ng/ml; BT474, 11,800 antibodies/cell, IC50 73.98 ng/ml).

387

388

389

390

391

392

393

394

395

396

397

398

399

400

401

402

403

404

405

406

407

408

409

410

411

412

413

414

415

416

417

Antibody ch10D7 is effective at delivering payloads for *in vivo* detection and treatment of xenograft models of primary TNBC

We next assessed the capacity of ch10D7 to accumulate in CDCP1-expressing TNBC xenografts in mice and subsequently, the impact of ch10D7-MMAE on tumor burden and mouse survival. First, we performed PET-CT imaging of mice carrying mammary fat pad xenografts of the TNBC cell line MDA-MB-231, two published TNBC PDX models (ELX 11-26 and HCl-010) [43, 44] or the newly generated TNBC PDX BB-091. Breast cancer pathology was confirmed for each model by histological assessment of H&E-stained xenograft sections, and the level of expression of CDCP1, breast cancer biomarkers (HER2, ER, PR) and the proliferative marker Ki67 was determined by immunohistochemistry (Supplementary Fig. S4). We have previously demonstrated the specificity of antibody ch10D7 for CDCP1 in vivo by comparison of 89Zr-10D7 PET imaging of CDCP1-silenced versus wildtype patient-derived pancreatic cancer xenografts in mice [31], and fluorescence imaging of the accumulation of indocyaninegreen (ICG) labelled ch10D7 versus IgG-ICG in patient-derived ovarian cancer xenografts in mice including the ability of unlabelled ch10D7 to reduce ch10D7-ICG signal in tumors [30]. For the four breast cancer models examined in the current study. xenografted mice were injected with ⁸⁹Zr-ch10D7 (~2 MBq/mouse; radiochemical purity ≥98%) and to assess the specificity of ch10D7 for its target, 24 h earlier with either PBS or unlabelled antibody (**Fig. 3A**). PET-CT scans indicated that within 24 h. ⁸⁹Zr-ch10D7 accumulated strongly and selectively in all four TNBC xenografts, including three PDXs, with signal sustained at the 48 and 72 h timepoints (Supplementary Fig. S5). Mice preinjected 24 h earlier with unlabelled ch10D7, had much lower tumor 89Zr signal than mice pre-injected with PBS indicating that unlabelled ch10D7 competed with 89Zrch10D7 for binding to CDCP1 demonstrating the specificity of the antibody for its target (Fig. 3B and Supplementary Fig. S5). This was confirmed by quantitative biodistribution analysis from recovered tumors, tissues and bloods, which showed much higher signal in tumors recovered from PBS versus unlabelled ch10D7 injected mice (xenograft MDA-MB-231 27.0 % versus 11.5 % ID/g, PDX ELX 11-26 20.5 % versus 7.8

% ID/g, PDX BB-091 28.4 versus 7.3 % ID/g; PDX HCI-010 30.8 versus 7.6 % ID/g; **Fig. 3C**). In non-tumor sites, the presence of unlabelled ch10D7 resulted in higher ⁸⁹Zr signal in sites of blood circulation (ie. blood, heart, lung) while signal was unaffected or slightly lower in bone, GIT, kidney, liver, muscle and tail (**Fig. 3C**). These differences in accumulation in normal tissues may be attributable to the unlabelled antibody reducing binding of ⁸⁹Zr-ch10D7 to tumor-expressed CDCP1 or by modulating reticuloendothelial processes through the Fc region of the antibody, particularly in organs with high vascular content, as previously observed [48, 49].

Having demonstrated by PET-CT imaging the ability of ch10D7 to accumulate strongly in primary TNBC xenografts, we examined the impact of the cytotoxin-loaded antibody, ch10D7-MMAE, on tumor burden and survival in mice xenografted orthotopically with two different models. Mice carrying xenografts of MDA-MB-231 cells were treated with two doses two weeks apart of ch10D7-MMAE or PBS as vehicle, or weekly doses for four weeks of the chemotherapy carboplatin (Fig. 3D left). As shown in Fig. 3D (middle), treatments with ADC ch10D7-MMAE significantly reduced tumor burden which was uncontrolled by carboplatin or PBS. Kaplan-Meier analysis showed similarly impressive improvement in median survival from approximately 50 days for carboplatin treated and control mice increasing to 111 days for ch10D7-MMAE treated mice (Fig. 3D right). In mice xenografted with PDX ELX 11-26, treatments with ch10D7-MMAE every two weeks significantly reduced tumor burden and significantly improved survival compared with control mice that received only PBS (Fig. 3E). These results indicate that ch10D7 accumulates strongly in orthotopic models of TNBC and is effective at delivering the cytotoxic payload MMAE to significantly reduce tumor burden and increase survival in TNBC xenografted mice.

Antibody ch10D7 is effective at delivering payloads for *in vivo* detection and treatment of a metastatic model of TNBC

TNBC demonstrates a notable propensity for metastasis, resulting in poor clinical outcomes for patients, underscoring the critical need for improved detection and therapeutic modalities for patients with metastatic disease [50]. To assess the

effectiveness of CDCP1-directed agents to detect and treat TNBC metastasis (**Fig. 4A**), we established a model by injecting mice in the lateral tail vein with luciferase-labelled MDA-MB-231-luc cells which disseminate via the vasculature establishing lung tumors within seven days (**Fig. 4A**). PET-CT imaging of mice at 24, 48 and 120 h after administration of ⁸⁹Zr-ch10D7 showed sustained signal in lungs identifying CDCP1-expressing tumors (**Fig. 4B**). Quantitative biodistribution analysis of recovered organs, shown in **Fig. 4C** (*left*), demonstrates ⁸⁹Zr-ch10D7 accumulates significantly more in the tumor-bearing lungs of the treatment group in comparison to the control arm at 16.5 % ID/g versus 8.6 % ID/g. As shown in **Fig. 4C** (*right*), the % ID/g of the organs containing metastasis were correlated with the bioluminescence signal of the tumors, demonstrating that the level of accumulation of ⁸⁹Zr-ch10D7 in metastasis was proportional to the metastatic burden.

Ongoing growth of lung tumors was monitored by bioluminescent imaging and treatments commenced on randomised groups when average signal per mouse reached >10⁷ p/s/cm²/sr. Treatments were vehicle (PBS), carboplatin, IgG-MMAE, ch10D7-MMAE, IgG-MMAE and carboplatin, or ch10D7-MMAE and carboplatin (Fig. **4D**). Bioluminescence imaging of tumor burden on day 50 indicated that ch10D7-MMAE as a single agent and in combination with carboplatin eliminated MDA-MB-231-luc tumor burden (Supplementary Fig. S6A-B) and this was confirmed by quantitative analysis (Fig. 4E). In contrast, the controls including single agent carboplatin had negligible impact on tumor burden (Fig. 4E and Supplementary Fig. S6A-B). MicroCT analysis of lungs recovered at endpoint indicated extensive numbers of MDA-MB-231luc tumor nodules on the lung surface from control mice and mice treated with carboplatin and/or IgG-MMAE (Fig. 4F). In contrast, lungs from mice treated with ch10D7-MMAE or the combination of ch10D7-MMAE and carboplatin, had normal gross morphology (Fig. 4F). Detailed immunohistochemistry analyses indicated that the lungs of control mice and mice treated with carboplatin and/or IgG-MMAE had been overwhelmed by CDCP1-expressing malignant cells whereas malignant cells had been completely eliminated by ch10D7-MMAE as a single agent and in combination with carboplatin, leaving normal lung histology (Supplementary Fig. S7). Treatment with single agent ch10D7-MMAE or the combination of ch10D7-MMAE and carboplatin also

significantly reduced metastatic tumor burden in comparison with control and standard of care chemotherapy (**Fig. 4G**; *P*<0.05). Kaplan-Meier analysis showed similarly impressive improvement in median survival increasing from 60-70 days for control mice and mice treated with carboplatin and/or IgG-MMAE, to 104 days for mice treated with the CDCP1-targeting ADC ch10D7-MMAE, and 116 days for mice treated with the combination of this ADC and carboplatin (**Fig. 4H**).

485

486

487

488

489

490

491

492

493

494

495

496

497

498

499

500

501

502

503

504

505

506

507

508

479

480

481

482

483

484

CDCP1-targeting ADC ch10D7-MMAE improves the efficacy of the HER2-targeting ADC T-DM1 against HER2⁺ breast cancer *in vitro*

CDCP1 is commonly over-expressed in HER2⁺ breast cancers as shown in our cohort of 75 primary HER2⁺ tumors. CDCP1 levels were medium to high in 80% of cases (medium in 41.3% and high in 38.7%, Fig. 1D and 1E) and in an independent cohort, it was noted that the proportion of tumors positive for HER2 at the highest levels (3+) and also expressing CDCP1 increased from 12% of primary tumors to 30% of metastases [19]. This study also reported that HER2 and CDCP1 co-overexpression increases transformation ability, cell migration, and tumor formation in vivo, and enhances HER2 activation and downstream signalling in vitro [19]. Accordingly, as a precursor to assays in mice, we next examined whether the CDCP1-targeting ADC ch10D7-MMAE can improve the efficacy in vitro of the trastuzumab-derived HER2targeting ADC T-DM1. To first ensure that binding of each agent to its target receptor did not impact binding of the other agent to its receptor, we first performed flow cytometry analysis to assess competition between ch10D7 and trastuzumab. Analysis of the four breast cancer cell lines MDA-MB-231, MDA-MB-453, BT474 and MDA-MB-361, indicated that signals from ch10D7 and trastuzumab were additive, demonstrating that when applied in combination, each antibody is able to bind unhindered to its receptor target on the cancer cell surface (Fig. 5A).

In co-treatment assays, eight cell lines with known levels of cell surface HER2 and CDCP1 (**Supplementary Fig. S1A**), were treated with increasing concentrations of each ADC as single agents or the combination of both ADCs (0.125, 0.25, 0.5, 1 and 2 μ g/ml). Because residual tumor burden after treatment is a key driver of breast cancer

recurrence [51], to gain insight into whether co-treatment with the ADCs could reduce the risk of residual disease, for these assays we plotted treatment concentration versus the percentage of breast cancer cells remaining at the end of the treatment period, relative to vehicle-treated cells. As shown in **Fig. 5B-D**, there was significant variation in cell responses to ch10D7-MMAE and T-DM1, and to the combination of the two ADCs, with the lines able to be separated into three broad categories:1) two cell types particularly sensitive to single agent T-DM1; 2) three lines poorly responsive to single agent T-DM1 but at least partially sensitive to single agent ch10D7-MMAE; and 3) three lines with intermediate responsiveness to single agent T-DM1 that displayed increased sensitivity with the addition of ch10D7-MMAE.

Cells particularly sensitive to T-DM1 were the high HER2 expressers SKBR3 (626,000 anti-HER2 antibodies/cell) and HCC1954 (1,099,100 anti-HER2 antibodies/cell) cells (**Fig. 5B**). Because of low CDCP1 expression, cell death of the SKBR3 line was not increased by the combination of T-DM1 and ch10D7-MMAE; however, slightly increased death was seen in HCC1954 cells in response to the addition of ch10D7-MMAE, consistent with medium/high CDCP1 expression by this line (86,400 anti-CDCP1 antibodies/cell) (**Fig. 5B**).

The three lines poorly responsive to T-DM1 were the low HER2-expressing lines MDA-MB-231 (4,500 anti-HER2 antibodies/cell), MDA-MB-468 (310 anti-HER2 antibodies/cell), and T47D (30,000 anti-HER2 antibodies/cell) cells (**Fig. 5C**). Of these cells, only T47D cells, which express CDCP1 above the threshold of 27,000 anti-CDCP1 antibodies/cell, exhibited slightly increased cytotoxicity in the presence of the combination of T-DM1 and ch10D7-MMAE (**Fig. 5C**).

Interestingly, the remaining three lines, which also had medium to high levels of cell surface HER2 (MDA-MB-453 84,600 anti-HER2 antibodies/cell; BT474 992,500 anti-HER2 antibodies/cell; MDA-MB-361 343,800 anti-HER2 antibodies/cell), were not as sensitive to T-DM1 as SKBR3 and HCC1954 cells (**Fig. 5D**). However, each displayed increased cytotoxicity when T-DM1 was combined with ch10D7-MMAE. Also of note, of these three lines only MDA-MB-361 cells had cell surface CDCP1 expression above the threshold of 27,000 anti-CDCP1 antibodies/cell (**Fig. 5D**). Further assays are required to evaluate whether ch10D7-MMAE acts synergistically or additively with T-

DM1 against breast cancer. Taken together, the results suggest that ADC targeting of CDCP1 can be effective as a single agent against HER2-expressing breast cancers, and can also improve the efficacy of T-DM1, even for cells that express quite low levels of HER2 or CDCP1.

544

545

546

547

548

549

550

551

552

553

554

555

556

557

558

559

560

561

562

563

564

565

566

567

568

569

540

541

542

543

CDCP1-targeting ADC ch10D7-MMAE improves the efficacy of the HER2-targeting ADC T-DM1 against HER2⁺ breast cancer *in vivo*

To directly address whether a CDCP1-targeting ADC can improve the efficacy in vivo of targeting HER2, we evaluated ch10D7-MMAE in comparison and combination with T-DM1 in three in vivo models of breast cancer. The first two models recapitulate HER2-amplified breast cancer and the third model utilises tumors expressing low levels of HER2 (HER2^{low}) which is the more difficult to treat with HER2-targeting ADCs [52]. The first model employed HCC1954 cells which express high levels of CDCP1 and HER2 and were injected into the mouse vasculature to generate lung metastases (Fig. **6A**). Growth of HCC1954 cells in mouse lungs was quite slow and was controlled by three treatments with ch10D7-MMAE, T-DM1 or the combination of these two ADCs (5 mg/kg total protein/mouse/dose; Fig. 6B). At day 63 when the first mouse had to be sacrificed because of ill health, microCT analysis indicated that lungs recovered from control mice had extensive HCC1954 tumor nodules on the lung surface whereas lungs from mice treated with T-DM1, ch10D7-MMAE or the combination of T-DM1 and ch10D7-MMAE, had normal gross morphology (Fig. 6C). Kaplan-Meier analysis showed similarly impressive improvement in median survival increasing from 69 days for control mice to 168 days for mice treated with T-DM1, ch10D7-MMAE or the combination of T-DM1 and ch10D7-MMAE (Fig. 6D).

Impressive results were also obtained from mice orthotopically xenografted with PDX model ELX 14-06A which expresses HER2 and CDCP1 at high levels (**Supplementary Fig. S4**). Mice were treated with the same agents as mice xenografted with HCC1954 cells with the addition of a T-DM1/ch10D7-MMAE combination dosed at the same dose, not half the dose, of the individual ADCs (ie. 10 mg/kg total protein/mouse/dose) (**Fig. 6E**). During the course of the assay, T-DM1, ch10D7-MMAE

and the ADC combinations, caused a gradual reduction in tumor burden (**Fig. 6F**). Quantification at the end of the assay of recovered tumors confirmed the marked reduction in tumor burden caused by single and combination ADC treatments including a statistically significant reduction resulting from the higher 10 mg/kg/dose of the combination of T-DM1 and ch10D7-MMAE (**Fig. 6G**). Quantification of the weight of eight organs recovered from mice at the end of the assay, indicated that treatments with T-DM1, ch10D7-MMAE and the combination of these ADCs, including the highest combination dose of 10 mg/kg/dose, had no significant organ toxicities (**Supplementary Fig. S8**).

570

571

572

573

574

575

576

577

578

579

580

581

582

583

584

585

586

587

588

589

590

591

592

593

594

595

596

597

598

599

These results are suggestive that ADC targeting of CDCP1 could be an adjunct for breast cancers that have medium to high levels of tumor expressed CDCP1 and either show poor responses to existing HER2-targeted therapies or for whom these agents are poorly tolerated. To evaluate whether a CDCP1 targeting ADC could also be used to treat breast cancers expressing low levels of HER2 (HER2^{low}), we evaluated two doses of T-DM1, ch10D7-MMAE and the T-DM1/ch10D7-MMAE combinations (Fig. 6H) against orthotopic xenografts of MDA-MB-453 cells which express HER2 and CDCP1 at relatively low levels (84,600 anti-HER2 antibodies/cell, 27,000 anti-CDCP1 antibodies/cell; **Supplementary Fig. S1**). Interestingly, while tumor burden markedly decreased in response to ch10D7-MMAE, T-DM1 and the T-DM1/ch10D7-MMAE combination at 5 mg/kg (total protein dose), doses of the T-DM1/ch10D7-MMAE combination at 10 mg/kg (total protein dose) resulted in persistently undetectable tumor burden (Fig. 6I). Also of note, the higher dose T-DM1/ch10D7-MMAE combination treatment markedly improved survival from 135-146 days for ch10D7-MMAE, T-DM1 and the lower dose combination versus 200 days for the higher dose combination (Fig. **6J,** P<0.0001). Interestingly, immunohistochemical analysis of xenograft tumors recovered at the end of the experiment (ie. for all treatment groups except T-DM1/ch10D7-MMAE 10 mg/kg/dose) indicated that CDCP1 expression was retained after ch10D7-MMAE treatments, suggesting that it would be possible to administer additional doses of ch10D7-MMAE in the event of persistent disease or recurrence (Fig. 6K).

601

602

603

604

605

606

607

608

609

610

611

612

613

614

615

616

617

618

619

620

621

622

623

624

625

626

627

628

629

630

Downloaded from http://aacrjournals.org/clincancerres/article-pdf/doi/10.1158/1078-0432. CCR-24-2865/3536838/ccr-24-2865.pdf by University of New South Wales user on 05 February 2025

DISCUSSION

Our results suggest that molecular imaging agents directed against receptor CDCP1 have the potential to identify aggressive breast cancers for CDCP1 targeted treatments. In our patient cohorts, CDCP1 was present at a medium to high level on the surface of the malignant cells of a significant proportion of the poor performing breast cancer subtypes of TNBC (70%), HER2+ (80%) and metastatic ER+/HER2- (56-74%). A theranostic paradigm that first selects patients based on the detection of CDCP1 expressing tumors and then, for CDCP1-avid tumors, enables treatment with a CDCP1-targeted therapy could help improve outcomes for each of these breast cancers subtypes.

TNBCs constitute 10-20% of all breast cancers [50]. Single-agent chemotherapy remains the backbone of treatment for advanced TNBC, with newer targeted agents also in use such as immune checkpoint inhibitors and the Trop-2 targeting ADC sacituzumab govitecan. However, chemotherapy response rates are low [50] and longduration responses to targeted agents are also rare [10, 50, 53] which is not helped by the lack of biomarkers for patient selection [54]. Our results suggest that CDCP1 has potential as a target for treatment of TNBCs with 89Zr-ch10D7-PET imaging serving as a tool for identification of suitable patients. The situation is similar for HER2⁺ tumors which also constitute ~20% of all breast cancers. While HER2-targeted antibodies and more recently the ADCs T-DM1 and T-DXd have contributed considerably to improving patient outcomes, about 20% of patients experience recurrence and metastatic HER2⁺ breast cancer remains incurable [13, 55-61]. Our data demonstrate that ADC targeting of CDCP1 expressing HER2⁺ cells is as effective as T-DM1 against primary tumors and lung metastases in mice that express both receptors (HER2⁺ and CDCP1) at high levels. The results suggest that ADC targeting of CDCP1 could be an adjunct treatment for HER2⁺ breast cancers that have medium to high levels of tumor expressed CDCP1 and either show poor responses to existing HER2-targeted therapies or for whom these agents are poorly tolerated. Probably of greater significance is our finding that ch10D7-MMAE is as effective as T-DM1 against HER2⁺ xenografts expressing relatively low levels of HER2 and CDCP1 and that when used in combination, ch10D7-MMAE and T-

DM1 have impressive effects reducing tumor burden and improving survival. Furthermore, xenografts recovered from ch10D7-MMAE and T-DM1 treated mice maintain CDCP1 expression suggesting the possibility of administering additional and/or higher doses of ch10D7-MMAE in the event of persistent disease or recurrence. In fact, increasing the dose of the ch10D7-MMAE/T-DM1 combination from 5 to 10 mg/kg saw complete elimination of xenografts expressing relatively low levels of HER2 and CDCP1. The final group of patients that could potentially benefit from CDCP1 targeting is the ER⁺/HER2⁻ cohort which constitute a significant majority of breast cancers [62]. Patients with early-stage HR⁺/HER2⁻ disease most commonly experience significant long-term positive outcomes, while outcomes are also improving for advanced HR⁺/HER2⁻ cases in response to endocrine therapies, CDK4/6 and mTOR inhibitors, chemotherapy, and palliative and supportive care [63]. Our results indicating that the proportion of these cancers that are positive for CDCP1 increases from 44.9% in primary tumors to 56.4% in lymph node metastases and 74.3% in distant metastases. suggests that CDCP1 could be a suitable theranostic target to select patients with progressing ER⁺/HER2⁻ disease, for CDCP1-targeted treatment.

It should be noted that our immunohistochemical analysis showed higher proportions of some breast cancer cohorts positive for CDCP1 than previous studies. For example, we noted that 44.9% of primary ER⁺/HER2⁻, 80% of primary HER2 ⁺ and 69.7% of primary TNBC tumors had medium to high levels of CDCP1. Our results for the TNBC cohort are not dissimilar to results from two previous studies which both reported CDCP1 expression by 57% of primary TNBCs (n = 65 and 100 cases, respectively) [20, 21]. In contrast, CDCP1 expression was previously reported in only ~24% of 224 histologically undefined primary breast cancers although this increased to ~40% of non-matched metastases [19]. In another small cohort of 35 histologically undefined primary breast cancers, 57.5% had medium to high CDCP1 levels [29]. Differences between this study and the earlier studies may be due to differences in the antibody used, protocols or pre-analytical factors in tissue processing.

Our results also allow an estimation of the CDCP1 levels required for CDCP1targeted treatments to be effective as single agents and in combination with chemotherapy or targeted drugs. In our assays breast cancer cell lines were most sensitive in vitro to the CDCP1 targeting ADC ch10D7-MMAE when cell surface CDCP1 levels were above a threshold of 27,000 anti-CDCP1 antibodies/cell. When used in vivo. ch10D7-MMAE markedly improved the effectiveness of carboplatin chemotherapy against lung metastases of the TNBC cell line MDA-MB-231 which expresses cell surface CDCP1 at high levels. Although not as impressive as high expressing cells, cell surface CDCP1 levels as low as 11,800 anti-CDCP1 bodies/cell were able to mediate significant levels of ch10D7-MMAE induced cell killing in vitro as we noted in BT474 cells. In addition, in cells expressing relatively low levels of CDCP1, ch10D7-MMAE was able to markedly improve the effectiveness of the HER2-targeting ADC T-DM1 even when HER2 levels were quite low (eg. MDA-MB-453 cells 84,600 anti-HER antibodies/cell). This was supported by our in vivo data showing that the combination of ch10D7-MMAE and T-DM1 was more effective than each ADC at reducing the size of orthotopic xenografts in mice of MDA-MB-453 cells. Taken together, the results suggest that ADC targeting of CDCP1 can be effective as a single agent against breast cancers that have CDCP1 on the cell surface at >27,000 anti-CDCP1 antibodies/cell, but that when used in combination with other agents CDCP1-targeting ADCs could be effective against cell surface CDCP1 levels substantially lower than that threshold. In future experiments it will be important to examine whether CDCP1-targeted treatments act synergistically or additively with other treatments, including HER2-targeted ADCs.

662

663

664

665

666

667

668

669

670

671

672

673

674

675

676

677

678

679

680

681

682

683

684

685

686

687

688

689

690

691

692

In our *in vivo* experiments, no toxicities were noted in seven mouse organs. However, it is important to note that ADCs have been responsible for various organ toxicities in humans including ocular toxicity [64]. Accordingly, additional toxicity studies will be required, including in non-human primates, to understand the safety profile of ch10D7-MMAE. Furthermore, as single ADCs have been shown to cause toxicity, it is essential further investigations are undertaken to ensure suitable safety profiles when ADCs are administered in combination as we have done in our preclinical assays using ch10D7-MMAE and T-DM1.

In summary, this study demonstrates the potential of CDCP1 as a target to identify aggressive breast cancers for CDCP1-targeted therapy including TNBCs, and metastatic ER⁺ and treatment refractory/metastatic HER2⁺ tumors. Our results demonstrate that ⁸⁹Zr-labelled human/mouse chimeric antibody ch10D7 has potential to

- be effective for PET/CT imaging for selection of CDCP1-expressing breast cancers for
- treatment with a CDCP1-targeting ADC or therapeutic theranostic.

REFERENCES

695

- 696 1. Bray, F., et al., Global cancer statistics 2022: GLOBOCAN estimates of incidence 697 and mortality worldwide for 36 cancers in 185 countries. CA Cancer J Clin, 2024. 698 **74**(3): p. 229-263.
- Tapia, M., et al., Clinical Impact of New Treatment Strategies for HER2-Positive Metastatic Breast Cancer Patients with Resistance to Classical Anti-HER Therapies. Cancers (Basel), 2023. **15**(18).
- 702 3. Hou, Y., H. Nitta, and Z. Li, *HER2 Intratumoral Heterogeneity in Breast Cancer,* 703 an Evolving Concept. Cancers (Basel), 2023. **15**(10).
- 704 4. Yin, L., et al., *Triple-negative breast cancer molecular subtyping and treatment progress.* Breast Cancer Research, 2020. **22**(1): p. 61.
- 5. Gilardi, L., L.S. Airò Farulla, and F. Ceci, *Imaging for illuminating actionable pathways in breast cancer.* Curr Opin Oncol, 2022. **34**(6): p. 606-613.
- 708 6. Ndlovu, H., et al., *Imaging Molecular Targets and Metabolic Pathways in Breast* 709 *Cancer for Improved Clinical Management: Current Practice and Future* 710 *Perspectives.* Int J Mol Sci, 2024. **25**(3).
- 711 7. Shastry, M., et al., *Rise of Antibody-Drug Conjugates: The Present and Future.*712 American Society of Clinical Oncology Educational Book, 2023(43): p. e390094.
- 713 8. Qu, F., et al., Antibody-drug conjugates transform the outcome of individuals with low-HER2-expression advanced breast cancer. Cancer, 2024. **130**(S8): p. 1392-715 1402.
- 9. Gogia, P., et al., *Antibody-Drug Conjugates: A Review of Approved Drugs and Their Clinical Level of Evidence.* Cancers (Basel), 2023. **15**(15).
- 718 10. Shastry, M., et al., *Antibody-drug conjugates targeting TROP-2: Clinical development in metastatic breast cancer.* The Breast, 2022. **66**: p. 169-177.
- 720 11. Makawita, S. and F. Meric-Bernstam, *Antibody-Drug Conjugates: Patient and Treatment Selection.* American Society of Clinical Oncology Educational Book, 2020(40): p. 105-114.
- 723 12. Gough, M., et al., *Improved concordance of challenging human epidermal growth*724 *factor receptor 2 dual in-situ hybridisation cases with the use of a digital image*725 *analysis algorithm in breast cancer.* Histopathology, 2023. **83**(4): p. 647-656.
- 726 13. Swain, S.M., M. Shastry, and E. Hamilton, *Targeting HER2-positive breast cancer: advances and future directions.* Nature Reviews Drug Discovery, 2023. **22**(2): p. 101-126.
- 729 14. Li, A.C., al., Quantitative digital of HER2 et imaging analysis 730 immunohistochemistry predicts the response to anti-HER2 neoadjuvant 731 chemotherapy in HER2-positive breast carcinoma. Breast Cancer Res Treat, 732 2020. **180**(2): p. 321-329.
- 733 15. Wang, Y., et al., *Immunohistochemical HER2 score correlates with response to*734 *neoadjuvant chemotherapy in HER2-positive primary breast cancer.* Breast
 735 Cancer Res Treat, 2021. **186**(3): p. 667-676.

- 736 16. Wolff, A.C., et al., *Human Epidermal Growth Factor Receptor 2 Testing in Breast Cancer: ASCO–College of American Pathologists Guideline Update.* Journal of Clinical Oncology, 2023. **41**(22): p. 3867-3872.
- 739 17. Wen, Z., et al., *Deep Learning-Based H-Score Quantification of Immunohistochemistry-Stained Images.* Mod Pathol, 2024. **37**(2): p. 100398.
- 741 18. Duan, H., A. lagaru, and C.M. Aparici, *Radiotheranostics Precision Medicine in Nuclear Medicine and Molecular Imaging.* Nanotheranostics, 2022. **6**(1): p. 103-743 117.
- 744 19. Alajati, A., et al., *Interaction of CDCP1 with HER2 Enhances HER2-Driven* 745 *Tumorigenesis and Promotes Trastuzumab Resistance in Breast Cancer.* Cell 746 Reports, 2015. **11**(4): p. 564-576.
- Turdo, F., et al., *CDCP1* is a novel marker of the most aggressive human triplenegative breast cancers. Oncotarget, 2016. **7**(43): p. 69649-69665.
- 749 21. Forte, L., et al., *The PDGFRβ/ERK1/2 pathway regulates CDCP1 expression in triple-negative breast cancer.* BMC Cancer, 2018. **18**(1): p. 586.
- Zhao, J., et al., Overexpression of CDCP1 is Associated with Poor Prognosis and Enhanced Immune Checkpoints Expressions in Breast Cancer. J Oncol, 2022.
 p. 1469354.
- 754 23. Khan, T., et al., *The CDCP1 Signaling Hub: A Target for Cancer Detection and Therapeutic Intervention.* Cancer Research, 2021. **81**(9): p. 2259-2269.
- He, Y., et al., Proteolysis-induced N-terminal ectodomain shedding of the integral membrane glycoprotein CUB domain-containing protein 1 (CDCP1) is accompanied by tyrosine phosphorylation of its C-terminal domain and recruitment of Src and PKCdelta. J Biol Chem, 2010. **285**(34): p. 26162-73.
- 760 25. Wright, H.J., et al., *CDCP1 cleavage is necessary for homodimerization-induced migration of triple-negative breast cancer.* Oncogene, 2016. **35**(36): p. 4762-72.
- 762 26. Wright, H.J., et al., *CDCP1 drives triple-negative breast cancer metastasis* 763 through reduction of lipid-droplet abundance and stimulation of fatty acid 764 oxidation. Proc Natl Acad Sci U S A, 2017. **114**(32): p. E6556-e6565.
- 765 27. Law, M.E., et al., *Glucocorticoids and histone deacetylase inhibitors cooperate to block the invasiveness of basal-like breast cancer cells through novel mechanisms.* Oncogene, 2013. **32**(10): p. 1316-29.
- 768 28. Boyer, A.P., et al., *Quantitative proteomics with siRNA screening identifies novel*769 *mechanisms of trastuzumab resistance in HER2 amplified breast cancers.* Mol
 770 Cell Proteomics, 2013. **12**(1): p. 180-93.
- 771 29. Khan, T., et al., *CUB Domain-Containing Protein 1 (CDCP1) is a rational target* 772 for the development of imaging tracers and antibody-drug conjugates for cancer 773 detection and therapy. Theranostics, 2022. **12**(16): p. 6915-6930.
- 774 30. He, Y., et al., *Preclinical Evaluation of a Fluorescent Probe Targeting Receptor*775 *CDCP1 for Identification of Ovarian Cancer.* Mol Pharm, 2021. **18**(9): p. 3464776 3474.
- 777 31. Kryza, T., et al., *Effective targeting of intact and proteolysed CDCP1 for imaging* 778 and treatment of pancreatic ductal adenocarcinoma. Theranostics, 2020. **10**(9): 779 p. 4116-4133.

- 780 32. Snell, C.E., et al., *Improved relapse-free survival on aromatase inhibitors in breast cancer is associated with interaction between oestrogen receptor-α and progesterone receptor-b.* Br J Cancer, 2018. **119**(11): p. 1316-1325.
- 783 33. Dai, X., et al., Breast Cancer Cell Line Classification and Its Relevance with 784 Breast Tumor Subtyping. J Cancer, 2017. **8**(16): p. 3131-3141.
- 785 34. Vranic, S., Z. Gatalica, and Z.Y. Wang, *Update on the molecular profile of the MDA-MB-453 cell line as a model for apocrine breast carcinoma studies.* Oncol Lett, 2011. **2**(6): p. 1131-1137.
- 788 35. Kao, J., et al., *Molecular profiling of breast cancer cell lines defines relevant tumor models and provides a resource for cancer gene discovery.* PLoS One, 2009. **4**(7): p. e6146.
- 791 36. Riaz, M., et al., *miRNA expression profiling of 51 human breast cancer cell lines* 792 *reveals subtype and driver mutation-specific miRNAs.* Breast Cancer Res, 2013. 793 **15**(2): p. R33.
- 794 37. Neve, R.M., et al., *A collection of breast cancer cell lines for the study of functionally distinct cancer subtypes.* Cancer Cell, 2006. **10**(6): p. 515-27.
- 796 38. Hollestelle, A., et al., *Distinct gene mutation profiles among luminal-type and*797 basal-type breast cancer cell lines. Breast Cancer Res Treat, 2010. **121**(1): p.
 798 53-64.
- 799 39. Lacroix, M. and G. Leclercq, *Relevance of breast cancer cell lines as models for breast tumours: an update.* Breast Cancer Res Treat, 2004. **83**(3): p. 249-89.
- 801 40. Koch, M.K., et al., *Label-free isolation and cultivation of patient-matched human*802 *mammary epithelial and stromal cells from normal breast tissue.* Eur J Cell Biol,
 803 2021. **100**(7-8): p. 151187.
- Harrington, B.S., et al., *Cell line and patient-derived xenograft models reveal* elevated *CDCP1* as a target in high-grade serous ovarian cancer. Br J Cancer, 2016. **114**(4): p. 417-26.
- 42. Harrington, B.S., et al., *Anti-CDCP1 immuno-conjugates for detection and inhibition of ovarian cancer.* Theranostics, 2020. **10**(5): p. 2095-2114.
- 809 43. Chew, N.J., et al., *Evaluation of FGFR targeting in breast cancer through* 810 *interrogation of patient-derived models.* Breast Cancer Res, 2021. **23**(1): p. 82.
- 811 44. Deng, N., et al., Deep whole genome sequencing identifies recurrent genomic 812 alterations in commonly used breast cancer cell lines and patient-derived 813 xenograft models. Breast Cancer Research, 2022. **24**(1): p. 63.
- S14 45. Cuda, T.J., et al., *Preclinical Molecular PET-CT Imaging Targeting CDCP1 in Colorectal Cancer.* Contrast Media Mol Imaging, 2021. **2021**: p. 3153278.
- 816 46. Chopra, S., et al., *Theranostic Targeting of CUB Domain-Containing Protein 1*817 (CDCP1) in Multiple Subtypes of Bladder Cancer. Clin Cancer Res, 2023. **29**(7):
 818 p. 1232-1242.
- Tsuchikama, K., et al., *Exploring the next generation of antibody-drug conjugates*. Nat Rev Clin Oncol, 2024. **21**(3): p. 203-223.
- 48. James, B.H., et al., *The Contribution of Liver Sinusoidal Endothelial Cells to Clearance of Therapeutic Antibody.* Frontiers in Physiology, 2022. **12**.
- 823 49. Sharma, S.K., et al., *Influence of Fc Modifications and IgG Subclass on Biodistribution of Humanized Antibodies Targeting L1CAM.* J Nucl Med, 2022. 63(4): p. 629-636.

- 826 50. Bianchini, G., et al., *Treatment landscape of triple-negative breast cancer* expanded options, evolving needs. Nature Reviews Clinical Oncology, 2022. **19**(2): p. 91-113.
- 829 51. Medford, A.J., et al., *Molecular Residual Disease in Breast Cancer: Detection and Therapeutic Interception.* Clin Cancer Res, 2023. **29**(22): p. 4540-4548.
- Antonarelli, G., et al., *Management of patients with HER2-positive metastatic* breast cancer after trastuzumab deruxtecan failure. ESMO Open, 2023. **8**(4): p. 101608.
- 834 53. Bardia, A., et al., *Sacituzumab Govitecan in Metastatic Triple-Negative Breast Cancer.* New England Journal of Medicine, 2021. **384**(16): p. 1529-1541.
- Coates, J.T., et al., Parallel Genomic Alterations of Antigen and Payload Targets
 Mediate Polyclonal Acquired Clinical Resistance to Sacituzumab Govitecan in
 Triple-Negative Breast Cancer. Cancer Discovery, 2021. 11(10): p. 2436-2445.
- 839 55. Najjar, M.K., et al., *Antibody-Drug Conjugates for the Treatment of HER2-Positive Breast Cancer.* Genes (Basel), 2022. **13**(11).
- Ferraro, E., J.Z. Drago, and S. Modi, *Implementing antibody-drug conjugates* (ADCs) in HER2-positive breast cancer: state of the art and future directions.

 Breast Cancer Research, 2021. **23**(1): p. 84.
- 844 57. Burris, H.A., 3rd, et al., *Phase II study of the antibody drug conjugate* 845 *trastuzumab-DM1 for the treatment of human epidermal growth factor receptor 2* 846 *(HER2)-positive breast cancer after prior HER2-directed therapy.* J Clin Oncol, 847 2011. **29**(4): p. 398-405.
- Krop, I.E., et al., A phase II study of trastuzumab emtansine in patients with human epidermal growth factor receptor 2-positive metastatic breast cancer who were previously treated with trastuzumab, lapatinib, an anthracycline, a taxane, and capecitabine. J Clin Oncol, 2012. **30**(26): p. 3234-41.
- Filho, O.M., et al., *Impact of HER2 Heterogeneity on Treatment Response of Early-Stage HER2-Positive Breast Cancer: Phase II Neoadjuvant Clinical Trial of T-DM1 Combined with Pertuzumab.* Cancer Discov, 2021. **11**(10): p. 2474-2487.
- 855 60. Modi, S., et al., *Trastuzumab Deruxtecan in Previously Treated HER2-Low Advanced Breast Cancer.* New England Journal of Medicine, 2022. **387**(1): p. 9-857 20.
- 858 61. Zimmerman, B.S. and F.J. Esteva, *Next-Generation HER2-Targeted Antibody-*859 *Drug Conjugates in Breast Cancer.* Cancers (Basel), 2024. **16**(4).
- Huppert, L.A., et al., Systemic therapy for hormone receptor-positive/human epidermal growth factor receptor 2-negative early stage and metastatic breast cancer. CA: A Cancer Journal for Clinicians, 2023. **73**(5): p. 480-515.
- 863 63. Harbeck, N., et al., *Breast cancer.* Nat Rev Dis Primers, 2019. **5**(1): p. 66.
- 864 64. Eaton, J.S., et al., *Ocular Adverse Events Associated with Antibody-Drug* 865 *Conjugates in Human Clinical Trials.* J Ocul Pharmacol Ther, 2015. **31**(10): p. 589-604.

ACKNOWLEDGEMENTS

867

868

We acknowledge the Translational Research Institute for providing the core facilities that enabled this research, particularly the Biological Resources, Flow Cytometry,

Microscopy and Preclinical Imaging facilities. The Translational Research Institute is financially supported by the Australia Federal Government. We are grateful to all the patients who volunteered to take part in the Mater Breast Cancer Biobank and generously provided the tissue utilised in this study. We would like to thank Professor Alana L. Welm (Hunstman Cancer Institute, University of Utah, USA) for kindly providing resources (HCI-010 Breast Cancer PDX) for this study. We would like to thank Dr Edita Ritmejeryte and Dr Sarah Reed from Mass Spectrometry Facility, University of Queensland, Centre for Clinical Research, 71/ 918 Royal Brisbane and Women's Hospital, Herston, Queensland, 4029, Australia.

880

881

886

871

872

873

874

875

876

877

878

879

Funding

- This work was supported by grants from the NBCF (IIRS-085) to TK, and a higher
- degree scholarship awarded by The University of Queensland Graduate School (MG).
- 884 CES was supported by a Mater Foundation Betty McGrath Fellow and MG and JDH are
- supported by the Mater Foundation.

Ethics approval and consent to participate

- 887 Mouse experiments were performed in compliance with Australian laws on animal
- welfare. Mouse protocols were approved by the Animal Ethics Committee of the
- University of Queensland (MRI-UQ/470/10). For the retrospective ER+ TMA cohort, the
- use of clinical information and tumor blocks was approved by the Mater Health Services
- Human Research Ethics Committee with a waiver of consent (approval number: HREC/
- 15/MHS/123). The study was performed in accordance with the Declaration of Helsinki.
- 893 Experiments pertaining to human subjects, specifically regarding the use of breast
- cancer patient samples from the Mater Hospital, are covered by Mater Misericordiae Ltd
- 895 Human Research Ethics MML/35996 The Study of Breast Cancer and Related
- 896 Neoplasms.

897

Conflict of Interest Statement

- Yaowu He, Thomas Kryza and John D. Hooper are inventors on a patent covering the
- use of antibody 10D7 used in this study. No potential conflicts of interest were disclosed
- 900 by the other authors.

Author contributions

901

902

903

904

905

906

907

908

909

910

911

912

913

914

915

916

917

918

919

920

921

922

923

924

925

926

927928929930931932

M. Gough: Conceptualisation, resources, methodology, data curation, formal analysis, investigation, visualisation, writing-original draft, writing-review and editing. K.K.X. Kwah: resources, methodology, investigation, writing-review and editing. T. Khan: Conceptualisation, methodology, investigation, writing-review and editing. S. Ghosh: investigation, methodology, writing-review and editing. B. Sun: investigation, writingreview and editing. C.Y.J. Lee: investigation, visualisation, writing-review and editing. **K.A. Sokolowski:** resources, investigation, methodology, writing-review and editing. B.WC. Tse: resources, investigation, methodology, writing-review and editing. L. Wickramasuriya: investigation, writing-review and editing. K. Ferguson: resources, project administration, writing-review and editing. R. Rogers: resources, project administration, writing-review and editing. J.B. Goh: investigation, methodology, writingreview and editing. N.L. Fletcher: investigation, methodology, writing-review and editing. **Z.H. Houston:** investigation, methodology, writing-review and editing. **K.J. Thurecht:** resources, writing-review and editing. L.J. Bray: resources, investigation, methodology, writing-review and editing. C. Liu: investigation, data curation, formal analysis, writing-review and editing. C. Pyke: resources, project administration, writingreview and editing. E. Lim: resources, writing-review and editing. C.E. Snell: resources, data curation, formal analysis, writing-review and editing. Y. He: conceptualisation, resources, investigation, methodology, data curation, writing-review and editing. J.D. Hooper: conceptualisation, resources, data curation, visualisation, formal analysis, methodology, project administration, supervision, writing-review and editing. T. Kryza: conceptualisation, resources, methodology, investigation, visualisation, data curation, formal analysis, study supervision, project administration, writing-review and editing.

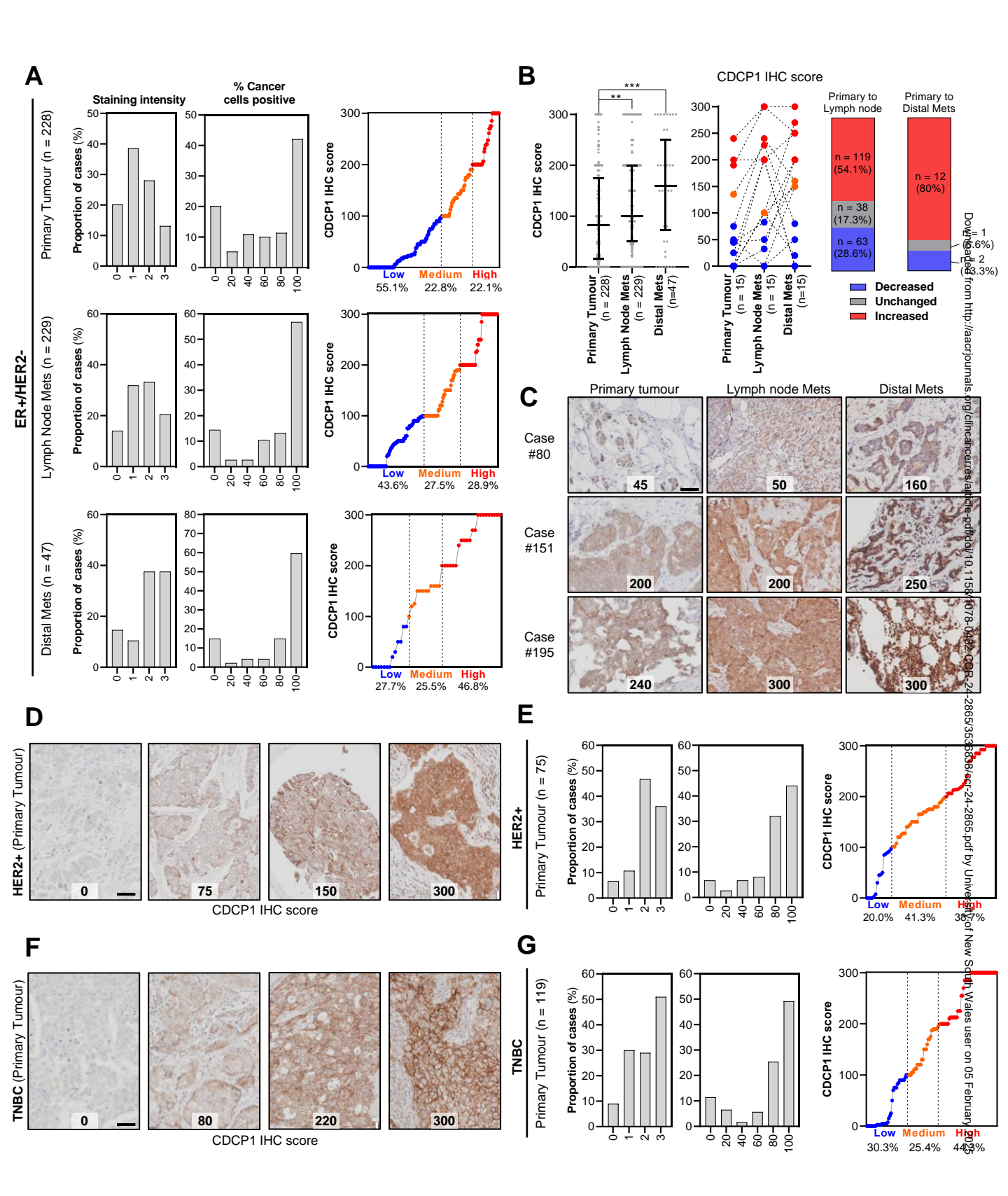


Figure 1: CDCP1 is highly expressed in HER2-positive and triple negative breast cancer subtypes, and is upregulated in the metastatic setting. CDCP1 protein expression in human breast cancer samples determined by immunohistochemistry using anti-CDCP1 antibody 4115. A) Graphs of scores for CDCP1 protein staining intensity (left) and percentage (%) cancer cell positive for CDCP1 protein (middle), and combined CDCP1 immunohistochemistry score (right) for ER+/HER2- breast cancer samples (top to bottom: primary, lymph node and distal metastasis). B) Change in CDCP1 protein expression between primary, lymph node and distal metastasis. Left: Change in CDCP1 IHC score in primary (n=228), lymph node (n=229) and distal metastasis (n=47) ER+, HER2- breast cancer. Data is represented as median with interguartile range. Overall statistical significance (****p<0.0001) was determined by Kruskal-Wallis test. Multiple comparisons between groups was performed using Dunn's multiple comparison test. Middle: Matched primary, lymph node and distal metastasis lesions plotted using CDCP1 IHC score. Right: Graphical representation of cases with increased (red), decreased (blue) or unchanged (grey). CDCP1 IHC expression in matched primary to lymph node tumours (left) and matched primary tumours to distal metastasis (right). C) Representative images of CDCP1 immunohistochemistry staining in matched ER+, HER2- primary (right), lymph node (middle) and distal metastasis (left) breast cancer lesions (Case #80, #151 and #195). Scale bar represents 50µm. D) Representative images of CDCP1 immunohistochemistry staining in HER2+ breast cancer (left to right): negative, weak, moderate and high intensity staining. Scale bar represents 50 µm. E) Graphs of scores for CDCP1 protein staining intensity (left) and percentage (%) cancer cell positive for CDCP1 protein (middle), and combined CDCP1 immunohistochemistry score (right) for HER2+ breast cancer. F) Representative images of CDCP1 immunohistochemistry staining in triple negative breast cancer (left to right): negative. weak, moderate and high intensity staining. Scale bar represents 50 µm. G) Graphs of scores for CDCP1 protein staining intensity (left) and percentage (%) cancer cell positive for CDCP1 protein (*middle*), and combined CDCP1 immunohistochemistry score (*right*) for triple negative breast cancer.

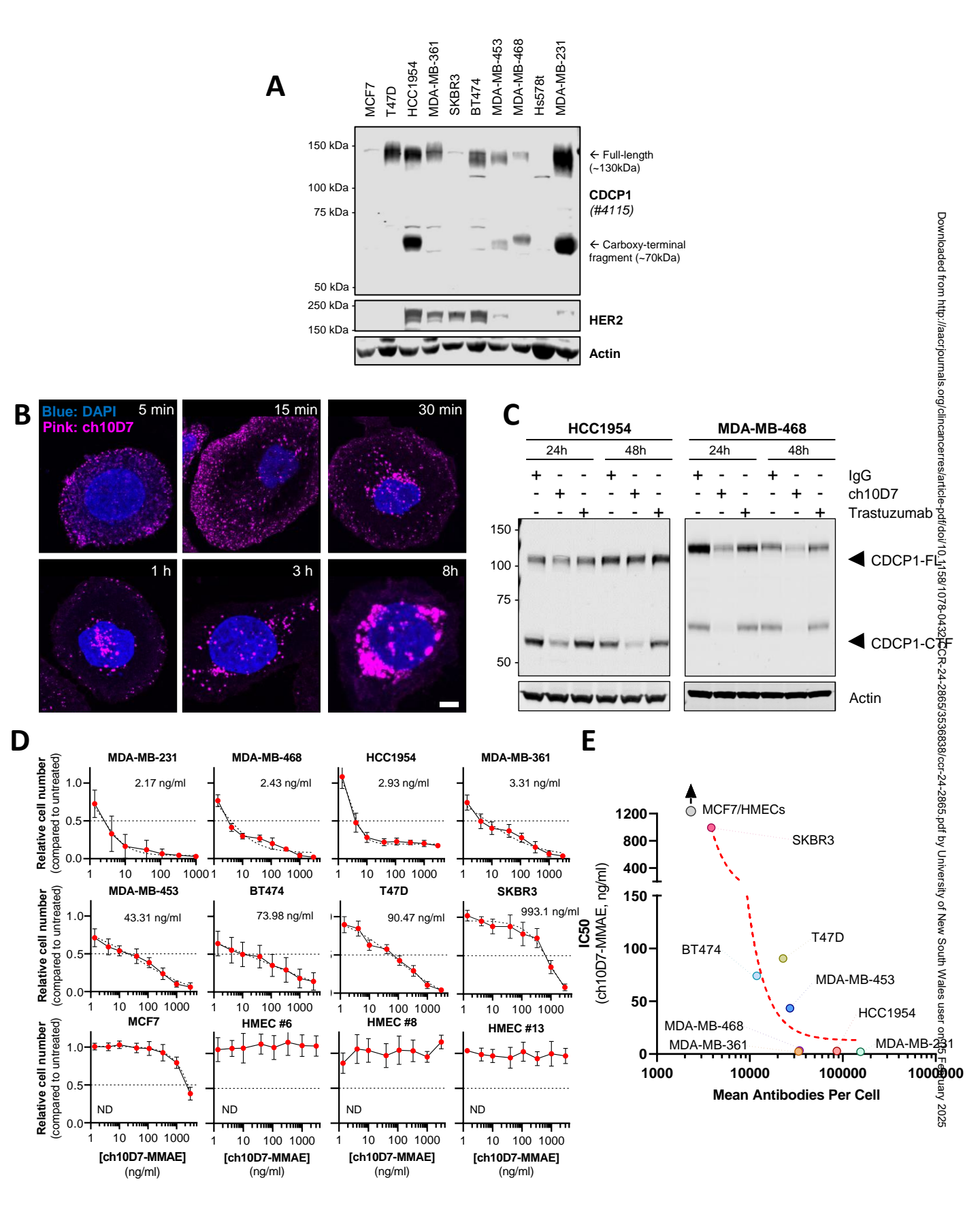


Figure 2

Downloaded from http://aacrjournals.org/clincancerres/article-pdf/doi/10.1158/1078-0432. CCR-24-2865/3536838/ccr-24-2865.pdf by University of New South Wales user on 05 February 2025

Figure 2: Antibody ch10D7 induces receptor internalisation and degradation.

A) Western blot analysis of total CDCP1 and HER2 expression in lysates from ten breast cancer cell lines. Lysates were probed by western blot analysis for CDCP1 (antibody 4115), HER2 (antibody 29D8), and Actin. B) Qualitative confocal imaging of CDCP1 receptor internalization (5 mins – 8 h) following treatment with ch10D7 (5 μg/ml), binding to CDCP1 on HCC1954 cells. Cells were plated, treated for indicated time points and fixed with PFA, followed by permeabilization and visualization using secondary antibody (Alexa Fluor 647 Anti-Human, pink) and counterstained with DAPI (DNA, blue). White scale bar represents 20 µm. C) Impact of anti-CDCP1 antibody on CDCP1 expression in two breast cancer cell lines, HCC1954 and MDA-MB-468. Western blot analysis of lysates from cell lines treated for 24 or 48 h with control IgG, ch10D7 or Trastuzumab (5 µg/ml). Lysates were probed by western blot analysis for CDCP1 (antibody 4115) and Actin. D) Quantitative analysis of cytotoxic activity of ch10D7-MMAE on breast cancer cell lines. Cancer cells (2,000 cells/well) were treated with ch10D7-MMAE (1.37e-3 to 3 µg/ml). Cell growth was quantified using live cell imaging taken every 2 hours for 7 days, using an Incucyte. Data are presented as mean of relative cell growth (compared to untreated cells) +/- SD from three independent experiments. ND indicates IC50 was 'not determined' due to incalculable or >1000 ng/ml. E) Examination of the correlation between cell surface CDCP1 and cell response to ADC ch10D7-MMAE. Plot shows the potency of ch10D7-MMAE ADC (represented by IC50 values for each cell line) versus the number of fluorescently labelled anti-CDCP1 antibodies bound/cell.

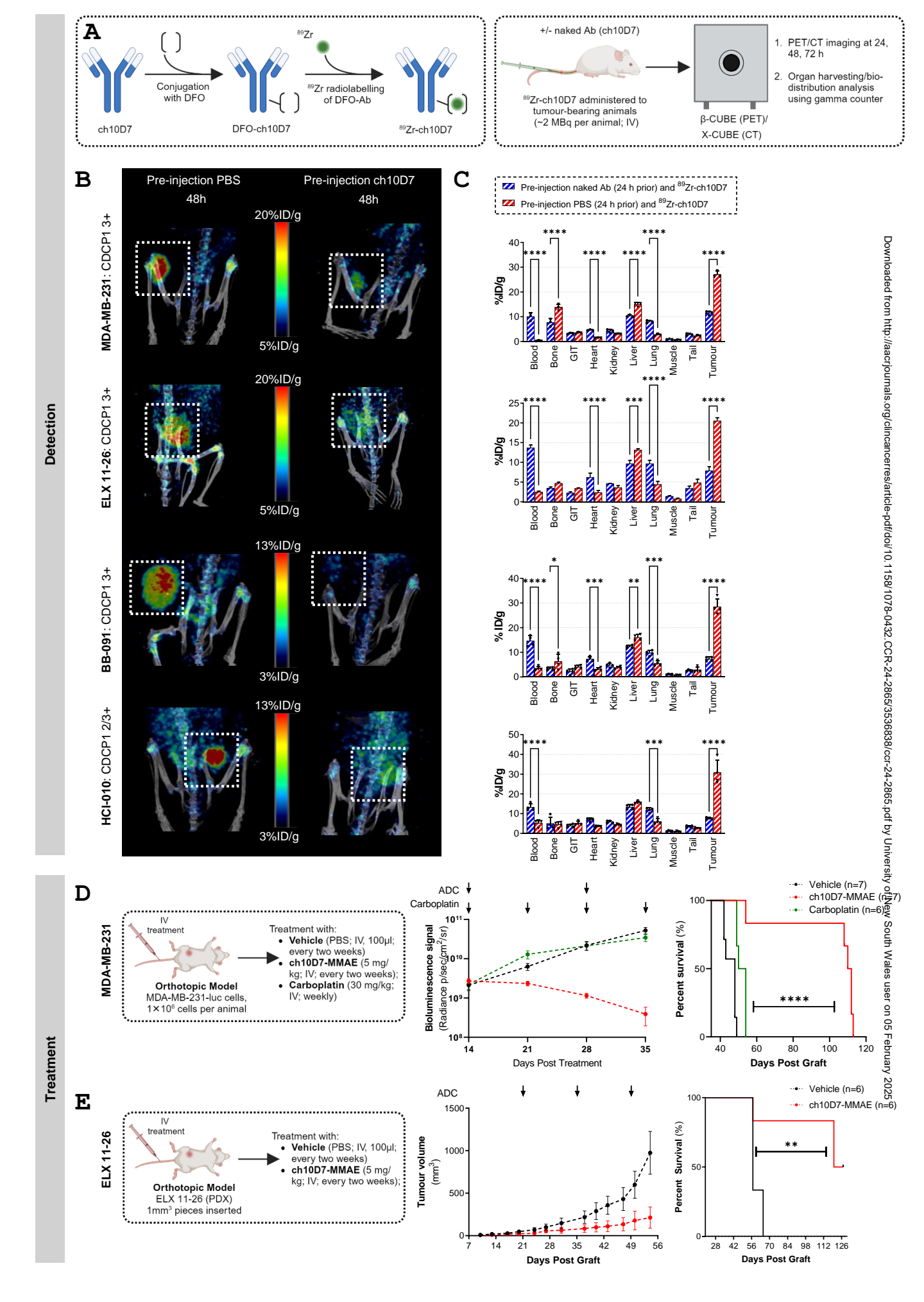


Figure 3

<u>Figure 3: Ch10D7 antibody demonstrates efficacy in the detection and treatment of triple negative breast cancer in preclinical models of primary disease</u>

Efficacy of 89Zr-ch10D7 in the detection of primary TNBC in vivo. A) Schematic depicting (left) generation of radiolabelled 89Zr-ch10D7 and (right) in vivo pipeline for evaluating ch10D7 as an imaging agent using PET-CT detection in orthotopic (mammary fat pad) models of TNBC. B) Representative PET-CT images of NSG mice carrying orthotopic xenografts of TNBC (top to bottom): MDA-MB-231 (injected activity 2.168 ± 0.086 MBq, range 2.07-2.3 MBq), ELX 11-26 (injected activity 1.553 ± 0.046 MBq, range 1.5-1.6 MBq), BB-091 (injected activity 2.106 ± 0.051 MBq, range 2.03-2.17 MBq) and HCl-010 (injected activity 2.118 ± 0.025 MBq, range 2.09-2.16 MBq). Mice underwent pre-injection with PBS (left column) and cold ch10D7 (right column) 24 h prior, followed by injection with 89Zr-\$\frac{1}{2}\$ ch10D7. C) Quantitative bio-distribution analysis of 89Zr-ch10D7 72 h post injection (top to bottom): MDA-MB-231 (n=6), ELX 11-26 (n=4), BB-091 (n=8) and HCl-010 (n=8). Measured by ex vivo radiometric analysis and displayed as %ID/g. *GIT sample contains uptake measured in spleen, stomach and bowel. Efficacy of ADC ch10D7-MMAE in the treatment of primary TNBC in vivo. Presented for each model: Left, schematic of the experimental protocol including xenograft site, cell line or PDX used, and treatment regimen; middle; graph of tumour burden vs time for each treatment group; left, Kaplan-Meier survival curve of mice. in each treatment group. **D)** Preclinical model of TNBC involving orthotopic xenografts in NSG mice of luciferase labelled MDA-MB-231 cells (1×106; 6-7 mice/group). Tumour burden was measured by weekly bioluminescent imaging. Mice were randomised then treated with ADCs every two weeks (5 mg/kg i.v.), weekly carboplatin (30 mg/kg i.v.) or vehicle control. E Preclinical model of TNBC involving orthotopic xenografts in NSG mice of patient-derived xenograft, ELX 11-26 (1mm³ pieces; 6 mice/group). Tumour burden was measured twice weekly using calipers. Mice were randomised then treated with ADCs every two weeks (5%) mg/kg i.v.) or vehicle control.

Days

··• Carboplatin+ch10D7-MMAE

Carboplatin+IgG-MMAE

Days post TVI

ch10D7-MMAE Carboplatin

Control

IgG-MMAE

+/- naked Ab (ch10D7)

Figure 4: ch10D7-MMAE is effective at reducing tumour burden in mice and limiting metastasis formation.

Efficacy of 89Zr-ch10D7 in the detection of metastatic TNBC in vivo. A) Schematic depicting (left) generation of radiolabelled 89Zr-ch10D7 and (right) in vivo pipeline for evaluating ch10D7 as an imaging agent (using PET-CT detection) in a metastatic model of TNBC using luciferase labelled cell line, MDA-MB-231. B) Representative PET-CT images of NSG mice carrying metastatic MDA-MB-231 tumours at 120 h. Mice underwent pre-injection with PBS (left column) and ch10D7 (right column), followed by injection with 89Zr-ch10D7 (injected activity 2.017 ± 0.144 MBq, range 1.77-2.17 MBq). **C)** Left, Quantitative bio distribution analysis of 89Zr-ch10D7 120 h post injection. Measured by ex vivo radiometris analysis and displayed as %ID/g. *GIT sample contains uptake measured in spleen, stomack and bowel. Statistical significance between different groups was performed using a two-way ANOVA test with **** p<0.0001. Right, Comparison of tumour bioluminescent radiance (provided in p/sec/cm²/sr) prior to PET-CT analysis vs %ID/g of the tumour measured using ex vivo radiometric analysis. Efficacy of ADC ch10D7-MMAE in the treatment of metastatic TNBC in vivo. D) Schematic of the experimental protocol including model, cell line used, and treatment regimen. E) Quantitative analysis of bioluminescent signal at day 50 from mice injected intravenously with MDA-MB-231 breast cancer cells and treated with PBS, IgG MMAE, ch10D7-MMAE, Carboplatin, Carboplatin + IgG-MMAE or Carboplatin + ch10D7 MMAE. Data shown as Mean ± SD. F) Micro-CT imaging of representative mouse lungs from each treatment group, sacrificed at day 50 to demonstrate comparative tumour burden. Great change of bioluminescent signal measured weekly for the duration of the experiments compared with signal at day 7. H) Kaplan-Meier Survival plot of mice following treatment. each treatment group, sacrificed at day 50 to demonstrate comparative tumour burden. G

Α			Mean Fluorescence Intensity						
	Cell Line	Secondary A	ntibody	ch10D7		Trastuzumab		ch10D7 + Trastuzumab	
	MDA-MB-231	2.57		1112		70.6		1188	
	MDA-MB-453	2.50		374		837		1206	
	BT474 5.31 MDA-MB-361 2.57			340		1163		1582	
				217		1609		1856	
B	lies/cell	SKBR3		HCC1954					
α-	-CDCP1 α-HER2	3,850 626,000		86,400 1,099,100					
α-	-CDCP1 α-HER2	MDA-MB-231 155,120 4,500 πs **	100 - 100 -	ns n	— 120 бо		00 00 ** ; † †	Ī.	
D	Nehide (hä/wil)		60- 40- 20-	T-DM (µg/ml)	60 40 20 20 20 20 0 0 0 0 0 0 0 0 0 0 0 0	Vehicle G-MMAE 0.05 5 12 2 0.125 5 22 1	7-DM1 Combo (µg/ml)	0.125	
α-	-CDCP1	27,000		11,800		34,2			
•	α-HER2		** ns	992,500	120 100 80 60 40		ns	·	

Vehicle (h8/wll) (9.0.25 (h8/wll) (125 (h8/w

0.5 0.25 0.125

T-DM1 (µg/ml) 0.5 0.25 0.125

(la/bh) LWG-L 0.255 0.125

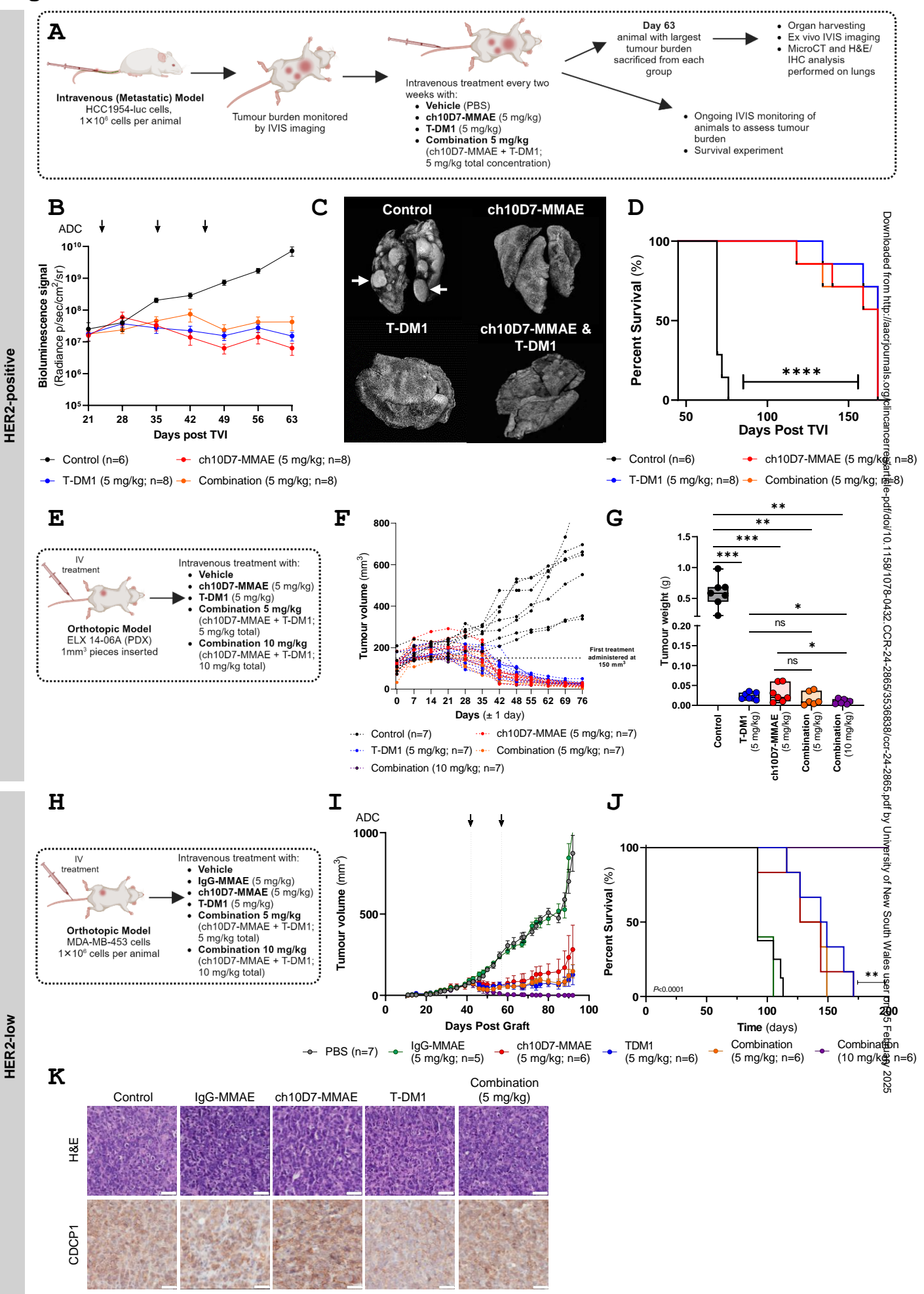
Vehide (hâ/ml) (hâ/ml) (hâ/ml) (hâ/ml) (hâ/ml) (ha/ml) (ha/ml)

Figure 5: Treatment of breast cancer with therapeutic HER2/CDCP1 co-targeting.

A) Flow cytometry analysis of MDA-MB-231, MDA-MB453, BT474 and MDA-MB-361

cells for CDCP1 and HER2 receptor availability using antibody ch10D7 (5 μ g/ml), trastuzumab (5 μ g/ml), and combination ch10D7+trastuzumab (saturating concentration of 10 μ g/ml total). Detection was performed using a secondary antibody, Invitrogen AlexaFluor 647 Goat Anti-Human (H+L). Data is presented as mean fluorescent intensity of at least 5,000 events. Number of antibodies bound per cell expressed as Mean \pm SD (x10³). **B-D)** Relative cell count of eight breast cancer cell lines treated for 12 h with increasing concentrations of ADCs (0.125 - 2 μ g/ml) then grown for a further 72 h in complete medium. Quantification was performed by assessment of PI staining using an Incucyte system.

Figure 6



Downloaded from http://aacrjournals.org/clincancerres/article-pdf/doi/10.1158/1078-0432. CCR-24-2865/3536838/ccr-24-2865.pdf by University of New South Wales user on 05 February 2025

Figure 6: Efficacy of ch10D7-MMAE in preclinical models of HER2-positive and HER2low breast cancer. A) Schematic of the in vivo pipeline for evaluating ch10D7 as a therapeutic agent in HER2-positive metastatic disease using a HER2-positive cell line (HCC1954-luc). B) Bioluminescent signal from mice injected intravenously with HCC1954-luc breast cancer cells, measured weekly for the duration of the experiment, with all treatment groups included. C) MicroCT imaging of representative mouse lungs from each treatment group sacrificed at day 63 (due to ethical endpoint of control animal) to demonstrate comparative tumour burden. D) Kaplan-Meier Survival plot of mice following treatment. **E)** Schematic of the *in vivo* pipeline for evaluating ch10D7 as a therapeutic agent in HER2-positive primary disease model using a PDX (ELX 14-06A). F) 1 mm3 pieces of ELX 14-06A tumour (HER2-positive) were implanted into the mammary fat pad of mice and allowed to grow until a tumour volume of 50 mm³ was reached. Following this, three treatments with PBS (control; n=7), ch10D7-MMAE (n=8), T-DM1 (n=7), Combination 5 mg/kg (n=7), Combination 10 mg/kg (n=7), respectively, were administered intravenously (fortnightly; 5mg/kg unless otherwise specified). Caliper measurements of the tumour were taken three times a week and plotted. G) Endpoint analysis of tumour weight for all animals. H) Schematic of the *in vivo* pipeline for evaluating ch10D7 as a therapeutic agent in HER2^{low} orthotopic model using a cell line xenograft (MDA-MB-453). I) Tumours were measured thrice weekly for the duration of the experiment, plotted with all treatment groups included. J) Survival plot of mice following treatment. K) H&E (top) and CDCP1 IHC (bottom) staining performed on harvested MDA-MB-453 tumour samples following two treatments with indicated agents. White scale bar represents 50µm.